Surface Science xxx (2016) xxx–xxx

Contents lists available at ScienceDirect

Surface Science

journal homepage: www.elsevier.com/locate/susc

Chemically selective formation of Si–O–Al on SiGe(110) and (001) for ALD nucleation using $H_2O_2(g)$

Sang Wook Park [a], Hyonwoong Kim [a], Evgueni Chagarov [b], Shariq Siddiqui [c], Bhagawan Sahu [c], Naomi Yoshida [d], Jessica Kachian [d], Randall Feenstra [e], Andrew C. Kummel [a,b,*]

[a] Materials Science and Engineering Program, University of California, San Diego, La Jolla, CA 92093, USA
[b] Department of Chemistry and Biochemistry, University of California, San Diego, La Jolla, CA 92093, USA
[c] TD Research, GLOBALFOUNDRIES USA Inc., 257 Fuller Road, Albany, NY 12203, USA
[d] Applied Materials, Inc., Santa Clara, CA 95054, USA
[e] Department of Physics, Carnegie Mellon University, Pittsburgh, PA 15213, USA

ARTICLE INFO

Article history:
Received 10 September 2015
Received in revised form 12 January 2016
Accepted 12 January 2016
Available online xxxx

Keywords:
Silicon–germanium
Scanning tunneling microscopy
Scanning tunneling spectroscopy
X-ray photoelectron spectroscopy
Atomic hydrogen
Atomic layer deposition

ABSTRACT

Passivation and functionalization via atomic hydrogen, hydrogen peroxide ($H_2O_2(g)$), and trimethylaluminum (TMA) on clean silicon–germanium ($Si_{0.5}Ge_{0.5}$(110) and $Si_{0.47}Ge_{0.53}$(001)) surfaces were studied and compared at the atomic level using ultra-high vacuum (UHV) scanning tunneling microscopy (STM), scanning tunneling spectroscopy (STS), and X-ray photoelectron spectroscopy (XPS) to understand the topological, electronic, and chemical structures of the surfaces. STM and XPS indicate that a sputter-cleaned SiGe(110) surface is terminated with adatoms, while a SiGe(001) surface is terminated with germanium dimers. STS demonstrates that the Fermi level on a clean SiGe(110) surface is pinned near mid-gap due to surface dangling bonds, while the Fermi level on a clean SiGe(001) surface is consistent with unpinning. A saturation dose of $H_2O_2(g)$ at 25 °C chemisorbs to SiGe surfaces, leaving the Fermi level at the surface consistent with unpinning, and the surface is functionalized mainly with Si–OH, Ge–OH, and Si–O–Ge bonds on both SiGe(110) and (001). After a subsequent TMA dose at 25 °C, XPS and STM verify that a thermally stable and well-ordered monolayer of Al_2O_3 is formed on SiGe(110) and (001) surfaces, resulting in the formation of Al–O–Si bonds. The $H_2O_2(g)$ functionalization provides three times more oxygen sites on the surface and three times as great a TMA nucleation density than does $H_2O(g)$ at both 25 °C and 120 °C. STS demonstrates that $H_2O_2(g)$- and TMA-dosed SiGe surfaces show a Fermi level consistent with unpinning and a local density of states (DOS) without any states between the conduction and valence band edge, indicating an ideal template for further atomic layer deposition (ALD) nucleation of high-*k* materials on SiGe(110) and (001) surfaces.

1. Introduction

With the decreasing size of complementary metal-oxide semiconductor (CMOS) devices, new structures and materials are required and have been investigated. “Fin” field-effect transistor (FinFET) devices are among of these new structures; they are three-dimensional and utilize multiple crystalline planes [1,2]. The multi-gate structure of a FinFET suppresses short-channel effects (SCEs) common to highly scaled, single-gate metal-oxide-semiconductor field-effect transistors (MOSFETs) [3,4]. For highly scaled devices, silicon-germanium (SiGe) is considered a promising material due to easy integration of strain engineering and higher mobility. The larger lattice constant of SiGe as compared to that of silicon (Si) alone can be employed to enhance electron mobility in n-channel metal-oxide-semiconductor (nMOS) transistors by applying biaxial tensile stress to the Si channel layers [5,6]. Additionally, the use of epitaxial SiGe materials in source-drain regions provides uniaxial compressive stress into the Si channel, thereby improving hole mobility in p-channel metal-oxide-semiconductor (pMOS) transistors [7]. The higher hole mobility of SiGe makes it a good alternative to Si for p-channel field-effect transistor (pFET) channels [8–10]. However, integration of SiGe as a channel material requires a clean and well-ordered surface for gate oxide deposition by suppressing GeO_x formation at the oxide/SiGe interface.

In order to employ SiGe as a channel material, a high quality interfacial layer between SiGe and a gate oxide needs to be formed [11]. Ge segregation to the surface of Si-capped Ge(001) pMOS transistors results in degraded device performance, such as low hole mobility and high interfacial trap density (D_{it}), due to the poor quality of Ge oxides [12]. Consequently, an oxide/SiGe interface with only Si atoms is expected to provide a better electronic structure.

* Corresponding author at: Department of Chemistry and Biochemistry, University of California, San Diego, La Jolla, CA 92093, USA. Tel.: +1 858 534 3368.
E-mail address: akummel@ucsd.edu (A.C. Kummel).

http://dx.doi.org/10.1016/j.susc.2016.01.009
0039-6028/

To form the improved interfacial layer with low defect density between gate oxides and channel surfaces, a proper passivation should be employed before the deposition of gate oxides [13]. Oxidation via ozone is known to passivate the Ge surface through the formation of GeO_2, thereby minimizing D_{it} [14]. Lee et al. [15] reported passivation of Ge(001) via H_2O eliminated dangling-bond states due to the termination of Ge atoms by hydroxyl groups (–OH) and –H. Recent studies have demonstrated that $H_2O_2(g)$ should be a good choice for passivating and functionalizing the SiGe surface with hydroxyls because the $H_2O_2(g)$ nucleation density is 3 times greater than that of $H_2O(g)$ on the Ge(001) surface [16]. Moreover, high coverage by hydroxyls is required to increase the gate oxide-nucleation density, thereby improving device performance (as indicated by low D_{it} and low on-state leakage).

Extensive studies have been performed to understand Si segregation on SiGe surfaces because its advantages for device performance. Chlorine plasma was reported to cause Si segregation on SiGe(001) surfaces via selective radical etching of Ge [17]. In addition, segregation of Si atoms on SiGe(001) surfaces by means of dichlorodifluoromethane (CF_2Cl_2) reactive-ion selective etching with directional etching characteristics has been reported [18]. Bestwick et al. [19] demonstrated that hydrogen bromide (HBr) plasma was effective for achieving a Si-rich SiGe surface by forming one monolayer of brominated Si on SiGe(001) again due to selective Ge etching [20].

An atomic hydrogen (H) dose at elevated temperatures generates Si segregation on Ge-covered Si(001) without preferential etching of Ge atoms. Rudkevich et al. [21] reported a "reversible exchange" between Ge and Si atoms on a Ge-covered Si(001) surface when the surface is exposed to atomic H at temperatures above 250 °C; based on discrete Fourier transform (DFT) calculations, the Si–H terminated surface has an energy that is 30 meV/atom lower than that of the Ge–H terminated surface. In addition, several studies have demonstrated the effectiveness of H in suppressing Ge segregation during SiGe epitaxial growth while leaving the surface terminated with hydrogen [22–24]. The Si–H bond being stronger than the Ge–H bond is considered to be the thermodynamic driving force segregating Si to the surface. An atomic H dose at substrate temperatures above 250 °C prevents the etching of Ge atoms on Ge(001) and Ge overlayers on Si(001) surfaces [25,26]. Moreover, an atomic H dose at 300 °C produces no etching of Si atoms on Si(001) [27]. Stesmans [28] reported hydrogen passivation provided a significant improvement in the reduction of the dangling bonds, thereby decreasing the density of interfacial states via the formation of Si–H bonds on the interface of Si/SiO_2.

While previous related studies had explained passivation of Ge(001) and SiGe(001) with $H_2O_2(g)$ [13,15,16], the focus of the present study is the unique passivation of SiGe(110) by $H_2O_2(g)$. The passivation of SiGe is distinct from Ge because of the –OH bonding, which induces surface segregation of Si atoms. The reaction of SiGe(110) with $H_2O_2(g)$ is distinct from the reaction of SiGe(001) with $H_2O_2(g)$ due to the SiGe(110) adatom chemistry and small domains of the SiGe(110) surface. This study seeks to understand and compare the chemical, topological, and electronic properties of SiGe(110) and (001) surfaces for the multi-gated device application; the surface chemistry of SiGe(110) is dominated by adatoms which pin the clean surface while the surface chemistry of SiGe(001) is dominated by surface dimers which unpin the clean surface. Passivation by means of atomic H and H_2O_2 is employed to unpin the Fermi level and induce formation of a Si-terminated SiGe(110) surface. Scanning tunneling microscopy (STM) and X-ray photoelectron spectroscopy (XPS) verify that atomic H produces the Si-segregated SiGe(110) surface while preventing etching. Functionalization by $H_2O_2(g)$ and a subsequent trimethylaluminum (TMA) dose with an anneal is utilized to maximize the nucleation sites for the high-k atomic layer deposition (ALD) process [29–31]. Compared to a $H_2O(g)$ dose, $H_2O_2(g)$ triples the nucleation density at both 25 °C and 120 °C. In the present report, each experimental process is explored using *in-situ* XPS, STM, and scanning tunneling spectroscopy (STS).

2. Experimental and computational details

2.1. Experimental details

P-type $Si_{0.47}Ge_{0.53}(001)$ films with 10^{17} cm^{-3} boron (B) doping grown on Si(001) wafers and p-type $Si_{0.5}Ge_{0.5}(110)$ films with 10^{15} cm^{-3} B doping grown on Si(110) wafers were supplied by GLOBALFOUNDRIES and diced into 12×5 mm^2 pieces. Samples were cleaned via repeated degreasing method using acetone, methanol, and deionized water, then dried with N_2 gas. Samples were loaded into a customized Omicron ultra-high vacuum (UHV) preparation chamber with a base pressure of 2×10^{-10} Torr, and cleaned via sputtering and annealing. The sputter process used a 1.5 kV argon ion (Ar^+) beam (Model 1403 ion gun, Nonsequitur Technologies) with a current of 1 μA and an Ar gas pressure of 6×10^{-7} Torr for 30 min, while the sample temperature was maintained at 500 °C via resistive pyrolytic boron nitride (PBN) heating. A 30-min annealing was performed at a sample temperature of 500 °C. After repeated sputter and annealing cycles, the chemical, topological, and electronic properties were verified via *in-situ* XPS, STM, and STS.

Sputter-cleaned SiGe(110) samples were exposed to atomic hydrogen in the UHV chamber using a thermal gas cracker (Atomic Hydrogen Source, Veeco). The gas pressure was controlled using a leak valve and measured through an ion gauge; the exposure was calculated in terms of Langmuirs (1 Langmuir (L) $= 1 \times 10^{-6}$ Torr · 1 s). The reported atomic H dose is based on the H_2 pressure, so the reported dose is the maximum possible dose. During the gas dose, the filament temperature of the thermal gas cracker was maintained between 1800 °C and 2200 °C, while the SiGe(001) and (110) samples were maintained at 300 °C; the cracking efficiency is expected to be 30%, but this could not be verified.

Samples were transferred to an *in-situ* ALD chamber with a base pressure of 2×10^{-8} Torr. $H_2O_2(g)$ and TMA were dosed at 25 °C without carrier gas by filling the dosing chamber with the precursor gas at 25 °C. Control experiments were also performed in which the substrate temperature was 120 °C for a $H_2O_2(g)$ dose. In order to perform a saturation dose on SiGe(001) and (110) surfaces, a 30% solution of $H_2O_2(aq)$ (Fisher Scientific) and TMA (98%, Strem Chemicals) were utilized. It was previously reported that a 30% solution of $H_2O_2(aq)$ results in a vapor of 2.67% $H_2O_2(g)$ at 25 °C [32]; therefore, the actual amount of $H_2O_2(g)$ participating in the chemical reaction should be smaller than the reported amount of $H_2O_2(g)$. Due to the possible reactivity of $H_2O_2(g)$ with stainless steel, the $H_2O_2(aq)$ solution was placed in a glass tube and dosed through a Teflon tube and Teflon valve to minimize the decomposition of $H_2O_2(g)$. Additionally, several cycles of $H_2O_2(g)$ were predosed to minimize the chemical reaction with the stainless-steel chamber walls before the samples were introduced to the chamber. The exposure pressures were measured with a convectron gauge and converted into Langmuirs.

After a dose with $H_2O_2(g)$ and/or TMA, samples were transferred to a UHV preparation chamber, followed by a post-deposition annealing at 300 °C. In order to determine the topological and electronic structures on the SiGe(001) and (110) surfaces after each treatment, the samples were transferred to an *in-situ* STM chamber (LT-STM, Omicron Nanotechnology) with a base pressure of 2×10^{-11} Torr. During the operation of the STM and STS at 25 °C, constant-current mode (I_{sp} = 200 pA) imaging was performed with a sample bias at −1.8 V to obtain filled-state STM images. Variable-z mode STS was performed using a modulation signal (0.1 V, 650 Hz) from an external lock-in amplifier (SR830 DSP, Stanford Research Systems) while sweeping the sample bias from −1.5 to +1.5 V and simultaneously moving the tip position forward then backward during the scan, so as to gain increased sensitivity to small currents that occur when the sample bias is close to zero volts [33,34]. The tip was modulated with 0.1 V_{ac} and the dI/dV was directly obtained from the lock-in measurement along with the I/V spectra. The I/V data was smoothed using a low-pass filter with energy

Please cite this article as: S.W. Park, et al., Chemically selective formation of Si–O–Al on SiGe(110) and (001) for ALD nucleation using H2O2(g), Surf. Sci. (2016), http://dx.doi.org/10.1016/j.susc.2016.01.009

width of (3.0 eV)/2π (frequency parameter value in filter of $(3.0\ \text{eV})^{-1}$), precisely as described in Fig. 7(b) of Ref. [35]. This procedure resulted in the formation of a broadened I/V, denoted as $\overline{I/V}$, which forms a suitable normalization quantity for dI/dV [35] (this same procedure was also used in prior work [13], although the description is more explicit in the current manuscript). The ratio $(dI/dV)/(\overline{I/V})$ has the property that band onsets show a *linear* dependence on voltage, so that they can be fit with a linear function in order to extract the band edge energies [35]. For accurate STS measurements, the $(dI/dV)/(\overline{I/V})$ from each measurement was rescaled from 0 to 1 and subsequently averaged from at least 6 individual spectra; this rescaled and averaged $(dI/dV)/(\overline{I/V})$ was plotted as a single spectrum in the STS figures. A fitting method was employed as described in previous STM/STS studies to extract the band edge energies for the $(dI/dV)/(\overline{I/V})$ spectra [35,36], with a linear function and including slight rounding at the onset due to both temperature and AC modulation. The onsets of the linear fits which correspond to the band gaps are calculated with error ranges. Simulated fits to the STS data are included in all STS figures as the dashed lines. The error ranges obtained from the fitting process are standard errors of the least-squares fits.

STS can rigorously show that surfaces are pinned by observation of n-type samples having a Fermi level below mid-gap and p-type samples having a Fermi level above mid-gap. However, to employ STS to rigorously prove unpinning, the Fermi level must be shown to have different positions on n-type and p-type samples. N-type SiGe(110) samples were not available; therefore, in this study "unpinned" means the data is only consistent with unpinning. Furthermore, on Ge(001) and $Si_{0.6}Ge_{0.4}$(001) surfaces, the STS Fermi level positions are never observed to be directly at the VB edge for p-type and the CB edge for n-type even on clean surfaces [13,15,16]; this may be due to intrinsic surface states. Furthermore, quantification of extrinsic surface states is best performed with other techniques such as D_{it} measurements on metal-oxide-semiconductor capacitors (MOSCAP)s.

Chemical analysis after each chemical step was performed with an *in-situ* monochromatic XPS (XM 1000 MkII/SPHERA, Omicron Nanotechnology). A constant analyzer-energy mode with a pass energy of 50 eV and a step width of 0.1 eV, using an Al Kα source (1486.7 eV), were utilized. The detection angle was 30° from the sample surface, which is close to the surface parallel, and an acceptance angle of +7° was utilized. For peak shape analysis, a CASA XPS v.2.3 was used through a Shirley background subtraction.

2.2. Computational details

The Density-Functional Theory (DFT) simulations were performed using a Vienna *ab-initio* simulation package (VASP) for plane-wave DFT simulation with projector augmented-wave (PAW) pseudopotentials [37–42] and a Perdew–Burke–Ernzerhof (PBE) exchange-correlation functional [43]. The SiGe was a regular polymorph with 50% Si and 50% Ge placed in checker-board pattern. The SiGe unit cell was optimized at variable volume with conjugate-gradient algorithm to avoid internal compression/strain. The optimized unit cell was later used to build the SiGe(110) supercell and initial slabs with the desired surfaces. The simulation box included ~12–15 Å of vacuum to avoid spurious interaction through periodic boundary conditions. All slab relaxations were performed using a conjugate-gradient relaxation algorithm with a force tolerance level of 0.05 eV/Å and a Gamma-centered 5 × 7 × 1 K-point grid. During relaxations, the 3 bottom layers of SiGe slabs were permanently fixed in their bulk-like positions and saturated with H atoms with 1 |e| charge to simulate continuous bulk. To avoid artificial field due to periodic boundary conditions, dipole correction in the vertical *z* direction was applied [39–41]. Due to high computational cost of these simulations including 116 atoms for the clean surface and 144 atoms for the hydroxylated, the 5 × 7 × 1 K-point set and the ~12 Å vacuum layer, the supercells were limited to 6 SiGe layers. Therefore, instead of modeling all the adatoms in multiple SiGe(110) adatoms structures, a simplified model was employed which retained the highest symmetry adatoms. The cross-sectional area of the simulated slabs is $15.90 \times 11.24\ \text{Å}^2$. More complex adatom patterns would require much larger cell sizes hardly affordable for DFT simulations. After relaxation, the final samples were rescaled to the higher accuracy Hey–Scuseria–Ernzerhof (HSE06) exchange-correlation functional lattice constant (different by ~1.1%) and the densities of states were calculated with the HSE06 functional [44–47]. The residual forces in HSE06 force field were inspected to verify that they were less than 0.05 eV/Å.

3. Results and discussion

3.1. Clean and H-passivated SiGe surfaces

$Si_{0.47}Ge_{0.53}$(001) and $Si_{0.5}Ge_{0.5}$(110) surfaces were prepared via repeated cycles of sputtering and annealing; afterwards, the cleanliness of the sputter-cleaned surfaces was verified via an *in-situ* XPS (not shown). The surface reconstructions were checked at the atomic level. Fig. 1 shows filled-state STM images of sputter-cleaned SiGe(001) and (110) surfaces, followed by 500 °C annealed surfaces. Based on previous studies, a clean SiGe(001) surface is known to be terminated with Ge dimers because of Ge segregation to the SiGe(001) surface [48–50]. In addition, based on a previous DFT simulation, a Ge dimer termination is known to be thermodynamically more stable than a Si dimer termination on clean SiGe(001) [13]. In Fig. 1(a) and (b), STM shows a surface reconstruction, mainly composed of dimers on SiGe(001), that is consistent with the schematic diagram in Fig. 1(c), and which is identical to the results of a previous study by Kaufman-Osborn et al. [13]. As shown in Fig. 1(d) and (e), SiGe(110) has a different surface reconstruction with smaller domains and increased disorder compared to the SiGe(001) surface with the same Si/Ge bulk ratio. In addition, the size of the atoms on SiGe(110) looks larger than SiGe(001) because the spacing of adatoms on SiGe(110) is larger compared to the row spacing of Ge dimers on SiGe(001). It is reported that Si and Ge(110) surfaces should have adatom reconstructions as shown by the schematic diagram in Fig. 1(f) to lower the surface energy by reducing the number of dangling bonds [51,52]; the number of dangling bonds in Fig. 1(f) is reduced by half in a unit cell due to adatom reconstructions. Note this is just one of many nearly degenerate adatom structures.

STS was employed to probe the surface electronic structures, because measurements of $(dI/dV)/(I/V)$ are known to be approximately proportional to the local density of states (LDOS) [33,34]. A clean n-type SiGe(001) surface is known to have an unpinned Fermi level positioned slightly above mid-gap in STS measurements [13]. The position of the Fermi level on a clean n-type SiGe(001) surface is the same as the position of the Fermi level on a clean n-type Ge(001) surface and a clean n-type Si(001) surface, and is consistent with a surface terminated by Ge dimers on SiGe(001) surface [16,53]. A Fermi level position consistent with unpinning was also observed on a clean p-type SiGe(001) surface because the Fermi level is close to the valence band (VB), as shown in Fig. 2(a). In contrast, a clean p-type SiGe(110) surface had a pinned Fermi level positioned near the mid-gap between the conduction and valence band edges, as shown in Fig. 2(a); this was consistent with the presence of surface adatoms with half-filled dangling bonds. The surface-pinning effect at the interface between substrate and gate oxides is known to cause undesirable device performance, such as high threshold voltage and subthreshold swing [54]. Therefore, the SiGe(110) surface needs to be unpinned by chemical passivation.

In order to passivate the SiGe(110) surface, atomic H was introduced to remove the dangling bonds. Atomic H was dosed at 3600 L on a sputter-cleaned SiGe(110) surface using a thermal gas cracker while the substrate temperature was maintained at 300 °C; the elevated temperature was employed to prevent Ge preferential etching. Fig. 2(a) shows STS measurements before and after an atomic H dose on a clean SiGe(110) surface. Six STS curves were taken at several positions and averaged into one curve, as shown in the graph of Fig. 2(a). Additionally,

Please cite this article as: S.W. Park, et al., Chemically selective formation of Si–O–Al on SiGe(110) and (001) for ALD nucleation using H2O2(*g*), Surf. Sci. (2016), http://dx.doi.org/10.1016/j.susc.2016.01.009

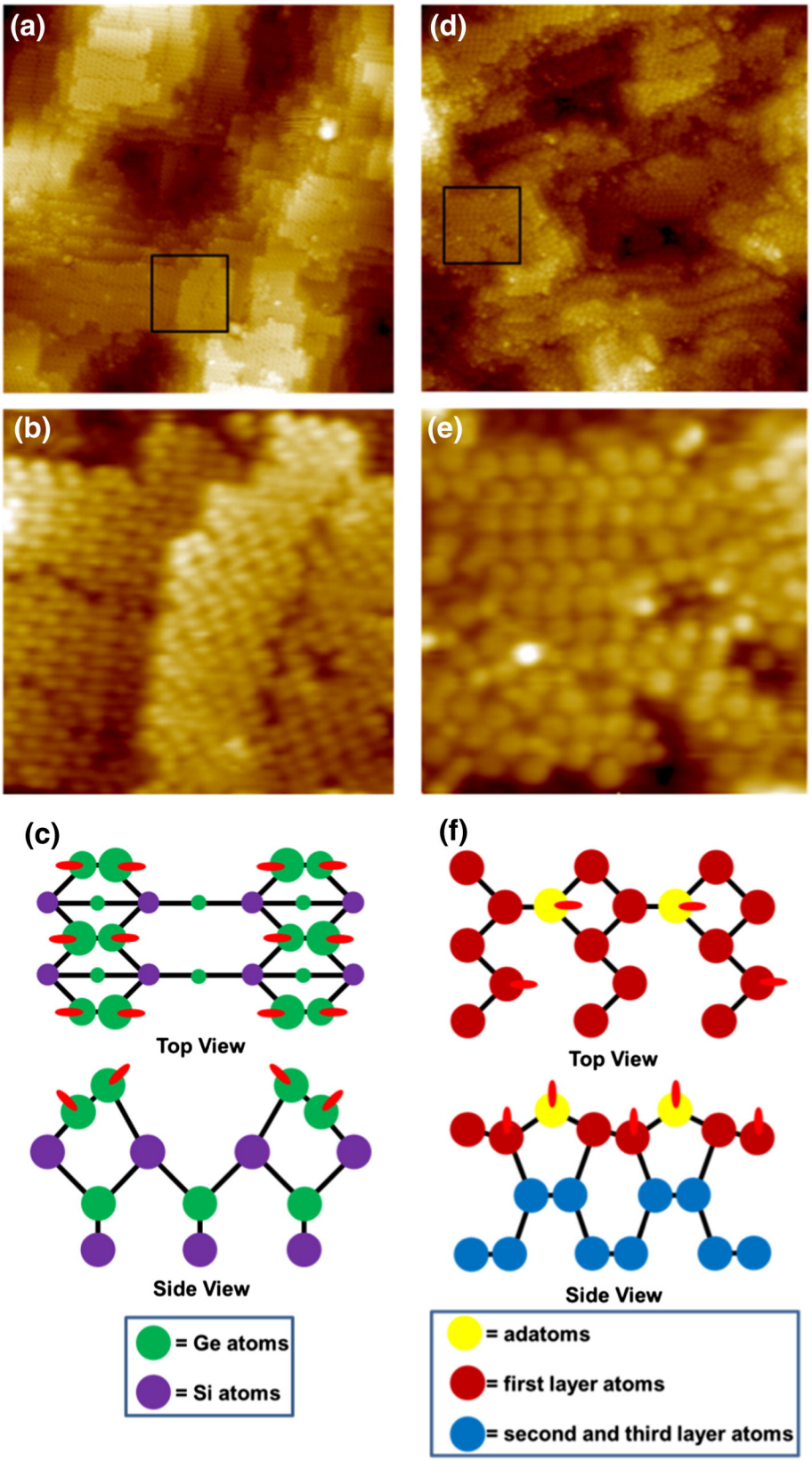

Fig. 1. STM images and proposed models of sputter-cleaned SiGe(001) and (110). (a) Filled state STM image (50×50 nm^2, $V_s = -1.8$ V, $I_t = 200$ pA) of sputter-cleaned and 500 °C annealed SiGe(001). A clean SiGe(001) surface is terminated with Ge dimers. (b) 10×10 nm^2 inset of a black square in (a) to show the surface reconstruction on SiGe(001). (c) Schematic diagram of Ge dimers on SiGe(001). (d) Filled state STM image (50×50 nm^2, $V_s = -1.8$ V, $I_t = 200$ pA) of sputter-cleaned and 500 °C annealed SiGe(110). A clean SiGe(110) surface is terminated with adatoms of both Si and Ge atoms. (e) 10×10 nm^2 inset of a black square in (d) to show the surface reconstruction on SiGe(110). (f) Schematic diagram of adatoms on SiGe(110).

Please cite this article as: S.W. Park, et al., Chemically selective formation of Si–O–Al on SiGe(110) and (001) for ALD nucleation using H2O2(g), Surf. Sci. (2016), http://dx.doi.org/10.1016/j.susc.2016.01.009

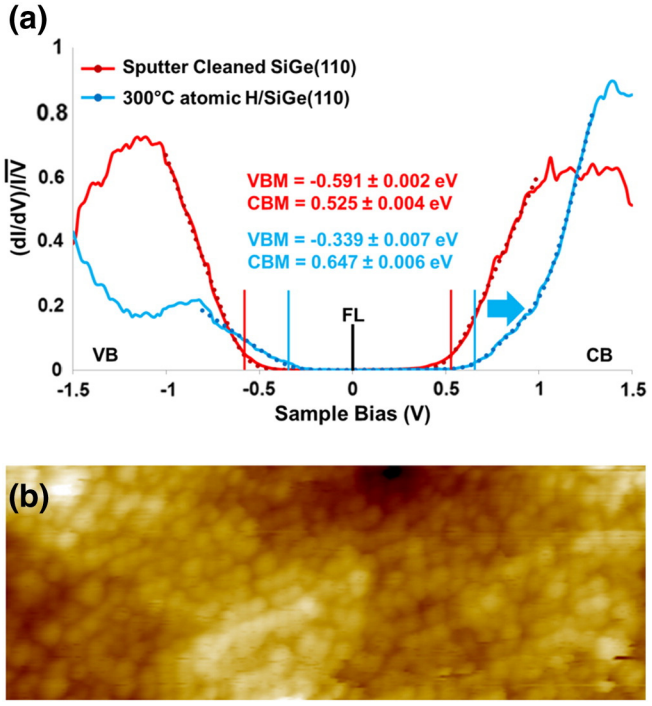

Fig. 2. STS and STM of 3600 L of atomic H dosed p-type SiGe(110) surface. (a) STS measurements of the p-type SiGe(110) surface before and after an atomic H dose at 300 °C. The Fermi level (FL) of the clean SiGe(110) surface (red curve) is pinned near the mid-gap, while the Fermi level of the atomic H dosed SiGe(110) surface (blue curve) is shifted towards the valence band edge, consistent with unpinning. Each STS curve is fit in order to determine the band gaps and Fermi level positions. The range of fitting is −1 to 1 V for sputter cleaned SiGe(110) surface and is −0.8 to 1.3 V for 300 °C atomic H/SiGe(110) surface. (b) Filled state STM image (40 × 15 nm^2, $V_s = -1.8$ V, $I_t =$ 200 pA) after an atomic H dose on a clean SiGe(110) surface. The atomic H produces a well-ordered surface structure and no etch pits are observed. (For interpretation of the references to color in this figure legend, the reader is referred to the web version of this article.)

curve fitting of the onsets of VB maximum (VBM) and CB minimum (CBM) were performed to quantitatively determine the band gaps and Fermi level positions [35,36]. Before the atomic H dose, the Fermi level was positioned near mid–gap, which is consistent with SiGe(110) being pinned by adatom dangling bonds. However, after the atomic H dose, the Fermi level was shifted toward the valence band edge (blue arrow). Since the substrate is p-type, the atomic H-dosed SiGe(110) surface having a Fermi level (0 V in STS) near the VB is consistent with unpinning. In Fig. 2(b), a filled-state STM image after an atomic H dose shows a uniform and ordered surface with an average row spacing of 7.9 Å, a standard deviation of 0.88 Å, and a standard error of 0.33 Å, as compared to an average row spacing of 8.1 Å on the clean surface, demonstrating that the adatoms are intact after an atomic H dose. In addition, there were no etch pits on the surface, which was consistent with the prevention of the Ge preferential etching.

3.2. $H_2O_2(g)$ dosed SiGe surfaces

In order to functionalize the SiGe(001) and (110) surfaces with hydroxyls, the clean surfaces were exposed to a 1.5×10^6 L dose of $H_2O_2(g)/H_2O(g)$ at 25 °C in an *in-situ* ALD chamber without any exposure to ambient air; note that this $H_2O_2(g)$ dose has a maximum value of 40,000 L. Note that the "$H_2O_2(g)$" dose refers to the dose with the $H_2O_2(g)/H_2O(g)$ mixture, but due to the high reactivity of $H_2O_2(g)$, the results are consistent with the surface functionalization being due to $H_2O_2(g)$, so the dose is denoted as "$H_2O_2(g)$". In a previous study, a SiGe(001) surface was shown to have all Ge surface atoms bonded to OH (HO–Ge–Ge–OH and HO–Ge–O–Ge–OH bonds) after exposure to a full saturation dose of $H_2O_2(g)$ at 25 °C [13]. Furthermore, the Ge–O_xH_y termination (Ge–O_xH_y included a mixture of Ge–OH and HO–Ge–O–Ge–OH sites) after $H_2O_2(g)$ was stable to at least 100 °C, in contrast to the combination of Ge–H and Ge–OH termination of Ge(001) from a H_2O dose [16].

Fig. 3 shows XPS spectra of Ge 3d and Si 2p peaks of the SiGe(110) surface after each chemical step. Sharp and asymmetric (due to spin-orbit splitting) Si and Ge peaks without any shoulders were observed on a sputter-cleaned SiGe(110) surface consistent with a clean surface; the peaks on clean surfaces showed resolved spin-orbit components consistent with previous studies [55,56]. In addition, the cleanness of the surface was verified as contaminant-free via XPS and STM analysis. In Fig. 3(a), while Si and Ge peaks on a clean surface contained only bulk-like components, a H_2O_2 dosed SiGe(110) surface had shoulder peaks at higher binding energy, corresponding to Si–O_xH_y and Ge–O_xH_y components. As shown in Fig. 3(b), the mixture of Si–O_xH_y and Ge–O_xH_y after a 25 °C H_2O_2 dose is consistent with Si and Ge atoms coexisting on a clean SiGe(110) surface, while a clean SiGe(001) is terminated with only Ge dimers.

After a dose at elevated temperature or annealing, atomic H induced a partial segregation of Si atoms to the surfaces. As shown in Fig. 3(c), 3,600 L of an atomic H dose at 300 °C generated sharp and asymmetric Si and Ge peaks without shoulder peaks, thereby verifying no adsorption of contaminants such as oxygen or hydrocarbons on the surface; the asymmetry was due to the preservation of the spin-orbit splitting, which was consistent with the conservation of a well-order surface. After the 300 °C atomic H dose, the Ge 3d and Si 2p peaks were shifted to higher binding energy compared to a sputter-cleaned surface; this was consistent with hydrogen termination at the surface, as shown in the previous report [57]; however, since the shift appears to be nearly equal for both Si and Ge, it is possible some of the shift is due to a change in the work function. Additionally, XPS confirmed the cleanness of the atomic H-dosed surface by showing no carbon and oxygen peaks. However, while the spectra of 25 °C $H_2O_2(g)$ that dosed the SiGe(110) surface without atomic H had both higher binding-energy shoulders on the Si and Ge peaks, as would be consistent with Si–O_xH_y and Ge–O_xH_y bonds, the spectra of 25 °C $H_2O_2(g)$ dosed SiGe(110) surface after a 300 °C atomic H dose primarily had a higher binding energy peak on Si in Fig. 3(d), consistent with preferential formation of Si–O_xH_y bonds.

The $H_2O_2(g)$ dose at 25 °C was reactive enough to form hydroxyl bonds on H-terminated SiGe surfaces, consistent with the following mechanism. For the mechanisms below, the reaction enthalpies were estimated using the polyatomic bonds enthalpies [58].

$$Si{-}H + H_2O_2(g) \rightarrow Si{-}OH + H_2O(g).$$

$$\Delta H = (293 + 210) - (368 + 497) = -362 \quad \text{kJ/mol}$$

or

$$Ge{-}H + H_2O_2(g) \rightarrow Ge{-}OH + H_2O(g)$$

$$\Delta H = (263 + 210) - (303 + 497) = -327 \quad \text{kJ/mol}$$

Since the estimated enthalpies of reaction are negative, the forward reactions are exothermic and are likely to occur. In addition, Bensliman et al. [59] demonstrated that a H_2O_2 dose onto hydrogen-terminated Si(111) surface eliminates Si–H bonds and results in oxidation of the surface as verified using Fourier transform infrared (FTIR) spectra. Based on a previous study, after a $H_2O_2(g)$ dose on SiGe(001), Ge dimers are bonded to two hydroxyls or two hydroxyls with an inserted bridge oxygen atom [13]. In comparison, H_2O_2 dosed SiGe(110) and 300 °C atomic H/SiGe(110) have different bonding configurations without dimer bonds, as shown by a proposed model in Fig. 4(a). Based on the crystallographic calculation, Si(001) has 6.8 atoms/nm^2 and the

Please cite this article as: S.W. Park, et al., Chemically selective formation of Si–O–Al on SiGe(110) and (001) for ALD nucleation using H2O2(g), Surf. Sci. (2016), http://dx.doi.org/10.1016/j.susc.2016.01.009

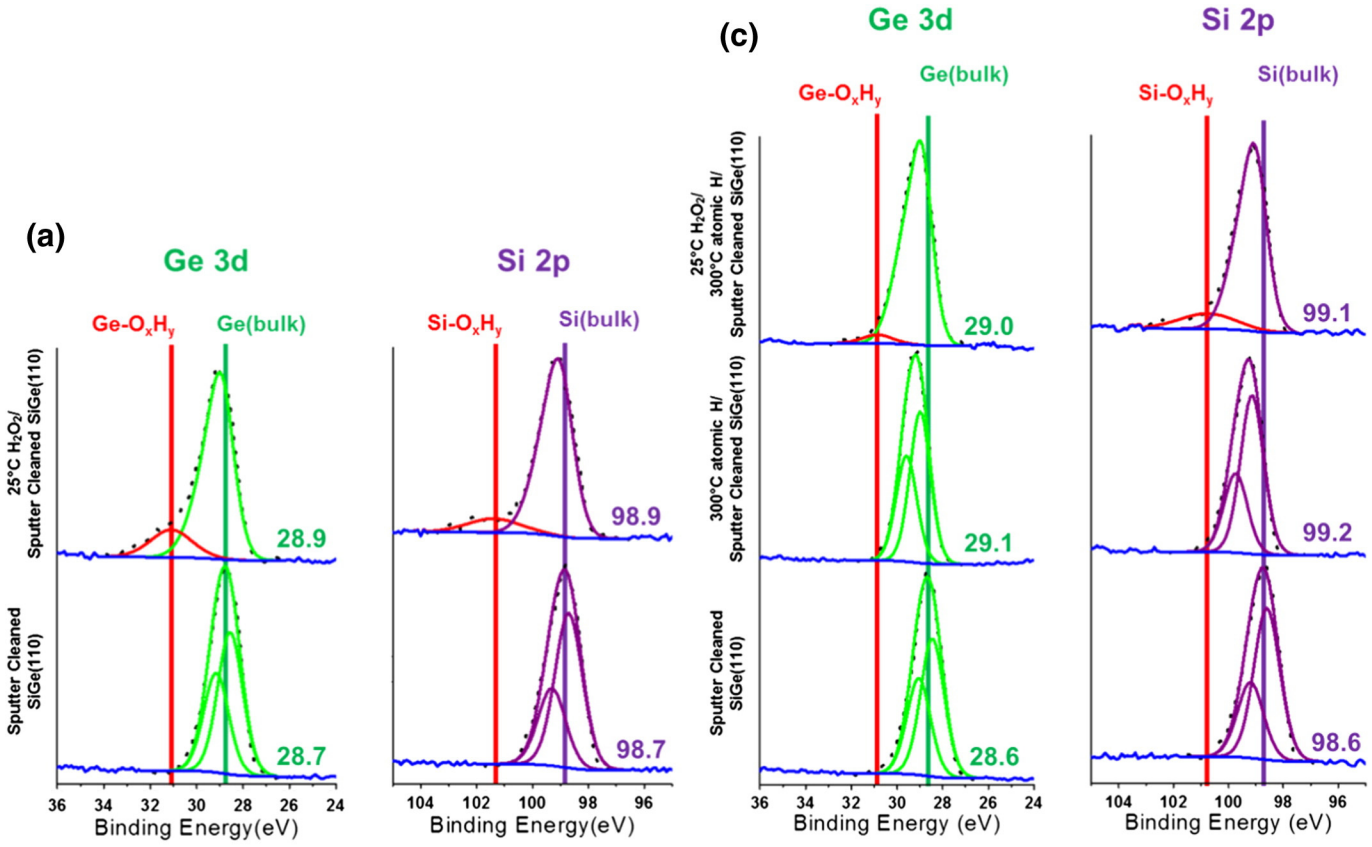

(b)

	GeO$_x$/Ge	SiO$_x$/Si
25°C H_2O_2/ Sputter Cleaned SiGe(110)	0.15±0.02	0.12±0.01
Sputter Cleaned SiGe(110)	0	0

(d)

	GeO$_x$/Ge	SiO$_x$/Si
25°C H_2O_2/300°C atomic H/ Sputter Cleaned SiGe(110)	0.03±0.01	0.13±0.01
300°C atomic H/ Sputter Cleaned SiGe(110)	0	0
Sputter Cleaned SiGe(110)	0	0

Fig. 3. Ge 3d and Si 2p peaks of H_2O_2/SiGe(110) surface with and without an atomic H dose. (a) Sputter-cleaned and 500 °C-annealed SiGe(110) Ge 3d and Si 2p peaks are composed of sharp and asymmetric bulk components with resolved spin-orbital components consistent with a clean surface without contaminants. When 1.5×10^6 L of $H_2O_2(g)/H_2O(g)$ containing a maximum of 40,000 L $H_2O_2(g)$ was dosed at 25 °C, XPS data without an atomic H dose showed Ge 3d and Si 2p peaks with shoulder peaks at higher binding energies, corresponding to Ge–O_xH_y and Si–O_xH_y components. (b) The table shows GeO$_x$/Ge and SiO$_x$/Si ratios on clean and 25 °C $H_2O_2(g)$/SiGe(110) surfaces. Similar ratios after $H_2O_2(g)$ dosing verify the coexistence of Si and Ge atoms on SiGe(110) surface. (c) XPS data after an atomic H dose at 300 °C show the change in the spectra in the Ge 3d and Si 2p peaks. After 3600 L of an atomic H dose at 300 °C, when $H_2O_2(g)$ was dosed at 25 °C, the surface was largely composed of Si–O_xH_y bonds, indicating a partial Si segregation to the SiGe(110) surface from the atomic H dose at 300 °C. The numerical values in the XPS spectra belong to the peak positions with an error rage of ±0.1 eV. (d) Table shows GeO$_x$/Ge and SiO$_x$/Si ratios after 300 °C atomic H. The higher ratio of SiO$_x$/Si verifies a partial Si segregation to the SiGe(110) surface. All errors are standard errors.

unreconstructed Si(110) has 9.6 atoms/nm^2, while the adatom-terminated Si(110) has 4.8 atoms/nm^2 because of 50% reduction of dangling bonds on the surface by adatoms [60]. It is assumed the ratio of spacings is identical on the corresponding SiGe(001) and SiGe(110) surfaces. To just remove the dangling bonds, the Si and Ge adatoms on SiGe(110) need only to be bonded to one hydroxyl group, forming Si–OH and Ge–OH bonds. However, for the O/(Si + Ge) ratio to be nearly identical on H_2O_2 dosed SiGe(001), SiGe(110), and 300 °C atomic H/SiGe(110), as shown in Fig. 4(b), the $H_2O_2(g)$ dose must partially remove the adatom reconstruction, or else there must be more oxygen insertion into adatom backbonds on SiGe(110) and 300 °C atomic H/SiGe(110) compared to oxygen insertion into surface dimers on SiGe(001).

In Fig. 4(b), XPS analysis of 25 °C H_2O_2/SiGe(001), 25 °C H_2O_2/SiGe(110), 120 °C H_2O_2/SiGe(110), 25 °C H_2O_2/300 °C atomic H/SiGe(110), and 25 °C H_2O/SiGe(110) are shown in terms of oxygen intensities normalized to Si 2p + Ge 3d peaks with standard error ranges of ±0.02. For the precise calculation of the ratios normalized to the SiGe surface, all XPS peaks were normalized by photoelectron cross-sections (Si 2p-0.817, Ge 3d-1.42, O 1 s-2.93) using the Hartree–Slater atomic model [61]. Compared to the 25 °C H_2O_2/SiGe(001) surface, the oxygen ratios of the 25 °C H_2O_2/SiGe(110), 120 °C H_2O_2/SiGe(110), and 25 °C H_2O_2/300 °C atomic H/SiGe(110) surfaces are nearly identical within error ranges, which was consistent with a high coverage of hydroxyls on SiGe(110) and 300 °C atomic H/SiGe(110) surfaces. The data are consistent with the 30% H_2O_2 partially removing the adatoms from SiGe(110), additional OH bonding at step edges or defects, or inducing significant oxygen backbond insertion, thereby equalizing the oxygen on SiGe(110) and SiGe(001). As shown in Fig. 3(a) and (c), the shoulder peaks after a $H_2O_2(g)$ dose on clean SiGe(110) and 300 °C atomic H/SiGe(110) are positioned between 100.5 eV and 101.5 eV for Si mostly corresponding to Si^{2+} (SiO), and between 30.5 eV and 31.5 eV for Ge mostly corresponding to Ge^{2+} (GeO), respectively. This demonstrates that the surface is composed

Please cite this article as: S.W. Park, et al., Chemically selective formation of Si–O–Al on SiGe(110) and (001) for ALD nucleation using H2O2(g), Surf. Sci. (2016), http://dx.doi.org/10.1016/j.susc.2016.01.009

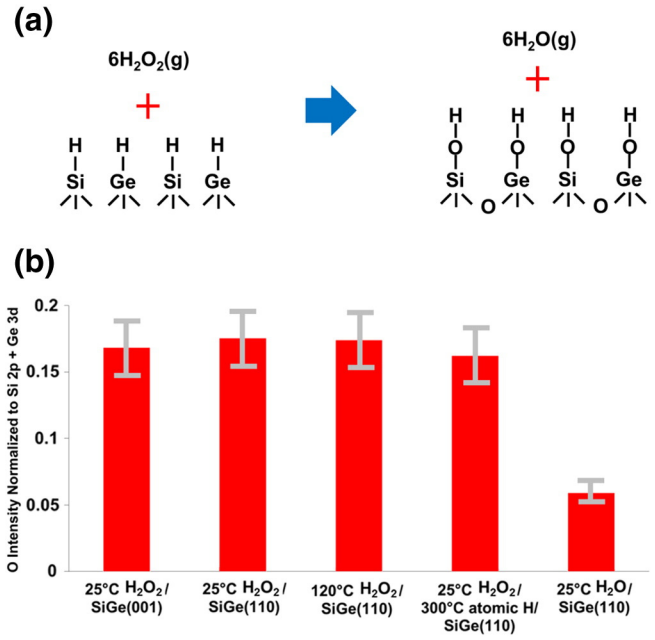

Fig. 4. Proposed model and XPS analysis of H_2O_2 dosed SiGe(001) and (110) surfaces. (a) Proposed dissociative chemisorption model of a 25 °C H_2O_2 dose on 300 °C atomic H/SiGe(110) surface. $H_2O_2(g)$ molecules dissociatively chemisorb onto hydrogens on SiGe(110) surface, forming surface hydroxyls and oxygen backbond insertion sites, and $H_2O(g)$ desorbs as a byproduct. (b) Intensities of O are normalized to Si 2p + Ge 3d peaks. After 25 and 120 °C $H_2O_2(g)$ doses on clean SiGe(001), (110), and 300 °C atomic H/SiGe(110) surfaces, the normalized intensities of O are almost the same within the error ranges, and greater than the intensity for 25 °C $H_2O(g)$/SiGe(110) surface. All errors are standard errors.

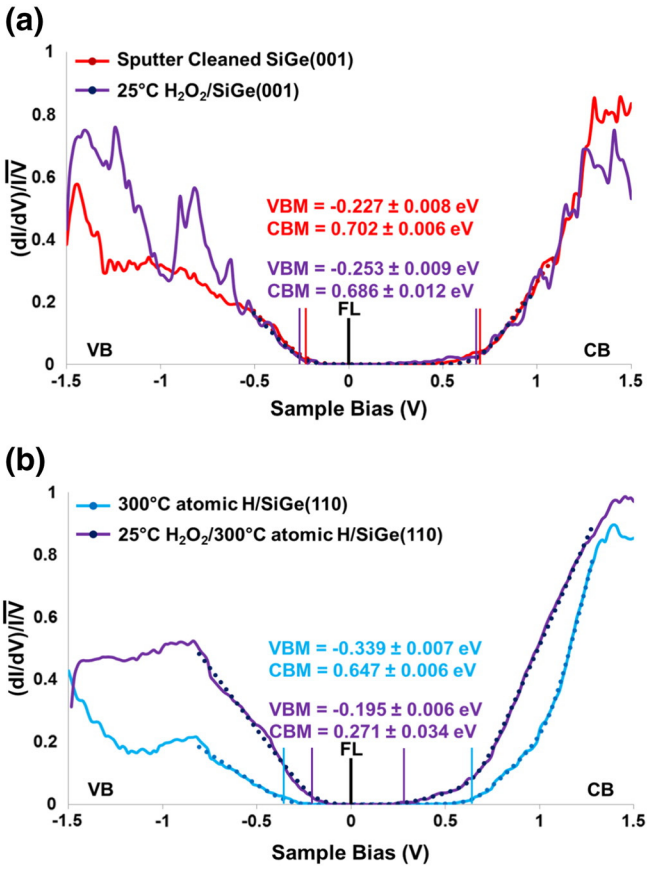

Fig. 5. STS measurements of H_2O_2 dosed p-type SiGe(001) and (110) surfaces. (a) STS measurements of the SiGe(001) surface before and after a H_2O_2 dose at 25 °C. The sputter-cleaned surface (red curve) is almost identical to the H_2O_2 dosed surface (purple curve). The range of fitting is −0.5 to 1.1 V for sputter cleaned SiGe(001) surface and is −0.5 to 1 V for 25 °C H_2O_2/SiGe(110) surface. (b) STS measurements of the 300 °C Atomic H/SiGe(110) surface before and after a H_2O_2 dose at 25 °C. Each STS curve is fit in order to determine the band gaps and Fermi level positions. The range of fitting is −0.8 to 1.3 V for 300 °C atomic H/SiGe(110) surface and is −0.8 to 1.3 V for 25 °C H_2O_2/300 °C atomic H/SiGe(110) surface. (For interpretation of the references to color in this figure legend, the reader is referred to the web version of this article.)

mostly of surface atoms with one hydroxyl and an oxygen inserted into a backbond or surface defects atoms (such as step edges) with bonds to two hydroxyls; each shoulder peak at higher binding energy has a wider full width at half maximum (FWHM) compared to a sputter-cleaned surface. This is consistent with a mixture of various surface states. It was previously shown that a 30% H_2O_2 dose results in a second site on Ge(001) and SiGe(001), which is HO–Ge–O–Ge–OH, containing two hydroxyls and an additional bridge oxygen on a Ge dimer [13,16]. On Ge(001), analysis of STM images shows these higher O-content sites are approximately 30% of all sites. In addition, based on the analysis of Ge 2p peaks, a H_2O_2 dose on 300 °C atomic H/SiGe(110) results in the formation of a higher binding energy component, corresponding to Ge–OH and X–O–Ge–OH bonding configurations consistent with an additional –OH binding site or an insertion of O into a Si–Ge or Ge–Ge bond. As explained in the supplement, the limited density of GeO_x and the small peak shift in the Ge 2p spectrum prevented definitive assignment of oxidation components Ge^{1+} and Ge^{2+} in the Ge 2p spectrum (see Supplementary information, Fig. S1). More importantly, the oxygen ratios for 25 °C H_2O_2/SiGe(110), 120 °C H_2O_2/SiGe(110), and 25 °C H_2O_2/300 °C atomic H/SiGe(110) are 3 times greater than for 25 °C H_2O/SiGe(110), consistent with a previous study [16]. This is largely because a 25 °C $H_2O(g)$ dose results in a mixture of less than a half monolayer of Si–OH and Ge–OH, and less than a half monolayer of Ge–H and Si–H, while a 25 °C $H_2O_2(g)$ dose results in a full monolayer of Si–O_xH_y and Ge–O_xH_y. Based on the model by Seah and Dench [62], the estimated escape depth of electrons in Si 2p and Ge 3d peaks is 1 nm with a detection angle of 30° from the sample surface and the estimated coverages of 17% of O/(Si + Ge) for 25 °C H_2O_2/SiGe(110) and 5% of O/(Si + Ge) for 25 °C H_2O/SiGe(110) correspond to 95% and 31%, respectively. These estimated coverages are calculated based on a simplified model in which the top monolayer on the surface is composed of oxygen atoms and the lower layers are composed of Si and Ge atoms; the attenuation of intensities is obtained through the formula $I = I_0 \exp(-t/\lambda)$ (I: intensity in the presence of the overlayer; I_0: intensity in the absence of any overlayer; t: thickness of the covering layer; λ: inelastic mean free path).

The electronic structures of 25 °C H_2O_2/SiGe(110) and 25 °C H_2O_2/300 °C atomic H/SiGe(110) surfaces were verified via the STS curves in Fig. 5. At least 6 STS curves were taken on different areas, and all the curves showed a consistent electronic structure. A previous study by Grassman et al. showed that when the p-type Ge(001) surface was exposed to O_2 at 25 °C, the STS spectra displayed the same Fermi level position as a sputter-cleaned Ge(001); since the surface was already p-type, the surface dipoles or acceptor surface states induced by an O_2 dose could not further move the Fermi level to the VB in STS measurements [63]. This phenomenon is consistent with the H_2O_2 dosed p-type SiGe(001) surface, which is terminated with Ge–O_xH_y bonds, and has a Fermi level near the VB in the STS measurements, as shown in Fig. 5(a). However, the 25 °C H_2O_2/300 °C atomic H/SiGe(110) surface (Fig 5(b)), which was composed of mainly Si–O_xH_y and partially Ge–O_xH_y bonds, showed a clear shift of the Fermi level in the STS measurements after a 25 °C H_2O_2 dose relative to the mid-gap position of the sputter-cleaned surface, and the position of the Fermi level was close to the VB, and similar to the H-terminated SiGe(110) surface. This is consistent with unpinning. It is noted that the bandgap decreased after a H_2O_2 dose on a 300 °C atomic H /SiGe(110) surface.

Please cite this article as: S.W. Park, et al., Chemically selective formation of Si–O–Al on SiGe(110) and (001) for ALD nucleation using H2O2(g), Surf. Sci. (2016), http://dx.doi.org/10.1016/j.susc.2016.01.009

3.3. TMA dosed SiGe surfaces

On the SiGe(001) and (110) surfaces that were functionalized by a 25 °C H_2O_2 dose, 1.5×10^5 L of TMA was subsequently dosed at 25 °C, followed by post-deposition annealing (PDA) at 300 °C for 20 min. In a previous report, when a TMA-dosed 25 °C H_2O_2/SiGe(001) surface was annealed at 300 °C, oxygen atoms that bonded to Ge atoms at the surface were completely transferred to Si atoms, forming Al–O–Si bonds. This is due to the stronger bond strength of Si–O bonds compared to Ge–O bonds [13]. Similarly, when TMA-dosed 25 °C H_2O_2/SiGe(110) and 25 °C H_2O_2/300 °C atomic H/SiGe(110) were annealed at 300 °C, the SiGe(110) surfaces were terminated with Al–O–Si bonds, as shown in Fig. 6. It is hypothesized that for 25 °C H_2O_2/SiGe(110), the thermal energy at 300 °C enables the Si atoms to diffuse to the surface to bond with O atoms, releasing Ge atoms to the subsurface on both SiGe(001) and (110).

A previous study on the SiGe(001) surface showed that the 25 °C TMA/25 °C H_2O_2/SiGe(001) surface showed no significant change in oxygen and aluminum ratios after 310 °C annealing, thus demonstrating the thermal stability of Al–O–Si bonds [13]. In order to understand the chemical compositions of the SiGe(110) surface, XPS analysis of 25 °C TMA/25 °C H_2O_2/300 °C atomic H/SiGe(110) before and after 300 °C PDA is shown in Fig. 7(a), with the carbon, oxygen, and aluminum intensities normalized to Si 2p + Ge 3d peaks (with error ranges of ±0.02). The ratio between Al and O was maintained 2:3 before and after PDA at 300 °C, while the C ratio decreased by 50%, as would be consistent with the desorption of methanes or ethanes. In addition, compared to a 25 °C $H_2O(g)$ dose, the 25 °C $H_2O_2(g)$ dose provided 3 times as great an oxygen ratio, indicating a higher nucleation density for high-k + H_2O_2 ALD process. One possible, simple model consistent with this data is that TMA molecules chemisorb dissociatively on both hydroxyls on the SiGe(110) surface and oxygen backbonded to adatoms, while methanes or ethanes desorb as byproducts, as shown in Fig. 7(b). This is consistent with a monolayer of stoichiometric Al_2O_3, indicating a thermal stability up to 300 °C.

Fig. 8 shows STM image and line trace analysis of SiGe(001) and (110) surfaces dosed with 25 °C $H_2O_2(g)$, subsequently dosed with 25 °C TMA, and annealed at 300 °C. The STM image of the 25 °C TMA/25 °C H_2O_2/SiGe(001) surface in Fig. 8(a) shows vertical rows along the direction of SiGe dimer rows, consistent with Al–O–Si bonds. In order to quantify the vertical rows structure, a line trace was performed in Fig. 8(b) at four different locations in the image. Each line in the analysis was measured at least 5 times. The line traces of the SiGe(001) surface have an average row spacing of 9.0 Å with a standard deviation of 1.1 Å and a standard error of 0.40 Å. The topological image and numerical analysis are almost identical to the results of a previous study [13]. In comparison, the STM image of 25 °C TMA/25 °C H_2O_2/300 °C atomic H/SiGe(110) surface shows different topological structures with lower surface order and larger row spacing in Fig. 8(c). The line traces of 25 °C TMA/25 °C H_2O_2/300 °C atomic

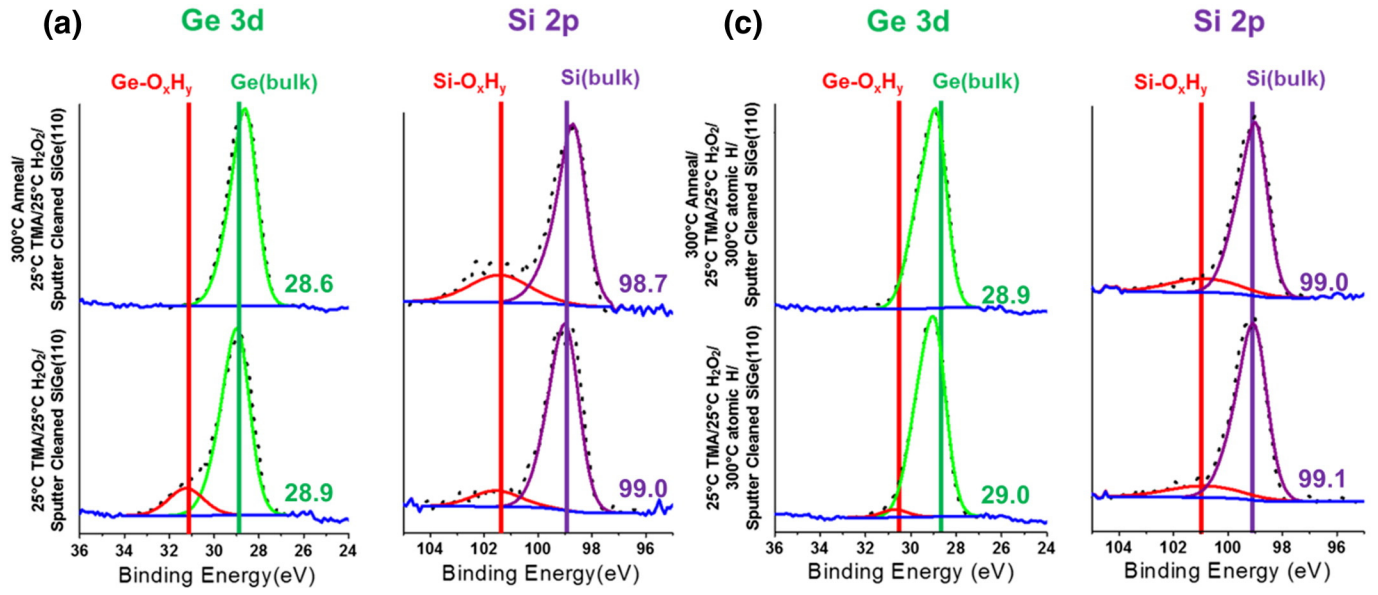

(b)

	GeO_x/Ge	SiO_x/Si
300°C Anneal/ 25°C TMA/25°C H_2O_2/ Sputter Cleaned SiGe(110)	0	0.21±0.03
25°C TMA/25°C H_2O_2/ Sputter Cleaned SiGe(110)	0.15±0.02	0.12±0.01

(d)

	GeO_x/Ge	SiO_x/Si
300°C Anneal/ 25°C TMA/25°C H_2O_2/ 300°C atomic H/ Sputter Cleaned SiGe(110)	0	0.16±0.02
25°C TMA/25°C H_2O_2/ 300°C atomic H/ Sputter Cleaned SiGe(110)	0.03±0.01	0.13±0.01

Fig. 6. Ge 3d and Si 2p peaks of TMA dosed SiGe(110) surface with and without an atomic H dose. (a) After a 25 °C TMA dose on the 25 °C H_2O_2/SiGe(110) surface, the Ge 3d and Si 2p peaks contain shoulder peaks corresponding to Al–O–Ge and Al–O–Si bonds. Annealing at 300 °C eliminates Al–O–Ge bonds and increases Al–O–Si bonds. (b) Table shows GeO_x/Ge and SiO_x/Si ratios without atomic H precleaning. Similar ratios verify the coexistence of Si and Ge atoms on the SiGe(110) surface prior to a H_2O_2 dose. Full Si termination requires H_2O_2 dose and annealing. (c) After a 25 °C TMA dose on 25 °C H_2O_2/300 °C atomic H/SiGe(110) surface, the surface is mainly composed of Al-O-Si bonds. After annealing at 300 °C, the surface is completely terminated with Al–O–Si bonds. The numerical values in XPS spectra are the peak positions with an error range of ±0.1 eV. (d) Table shows GeO_x/Ge and SiO_x/Si ratios with 300 °C atomic H. The higher ratio of SiO_x/Si verifies a partial Si segregation to the SiGe(110) surface after an atomic H dose. Full Si termination requires an H_2O_2 dose and annealing. All errors are standard errors.

Please cite this article as: S.W. Park, et al., Chemically selective formation of Si–O–Al on SiGe(110) and (001) for ALD nucleation using H2O2(g), Surf. Sci. (2016), http://dx.doi.org/10.1016/j.susc.2016.01.009

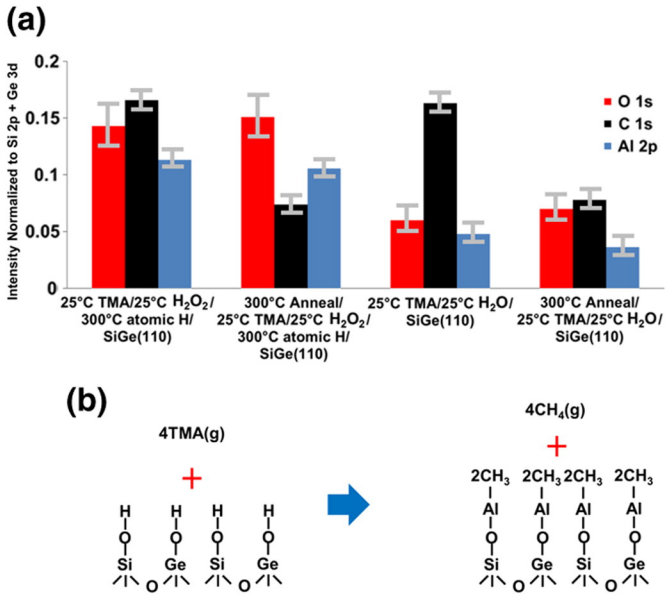

Fig. 7. XPS analysis and proposed model of dissociation mechanism of a TMA dosed SiGe(110) surface. (a) The intensities of O(red), C(black), and Al(blue) are normalized to Si 2p + Ge 3d peaks. After a TMA dose at 25 °C, the ratio between Al and O is 2:3, consistent with a stoichiometric monolayer of Al_2O_3. After annealing at 300 °C, the ratio between Al and O is nearly constant, consistent with thermal stability. The Al intensities after a 25 °C $H_2O_2(g)$ dose are 3 times greater than for a 25 °C $H_2O(g)$ dose, which is consistent with a nucleation density that is 3 times as great. All errors are standard errors. (b) Proposed dissociative chemisorption model of 25 °C TMA dose on 25 °C H_2O_2/300 °C Atomic H/SiGe(110) surface. TMA molecules dissociatively chemisorb onto hydroxyls on the SiGe(110) surface, with oxygen backbond insertion and methanes desorb as byproducts.

H/SiGe(110) surface in Fig. 8(d) have an average row spacing of 11.8 Å with a standard deviation of 1.2 Å and a standard error of 0.44 Å; the average spacing of the TMA products is slightly greater on SiGe(110) than on SiGe(001). The 11.8 Å average row spacing on SiGe(110) is almost 3/2 of the 8.1 Å adatom spacing on a clean SiGe(110), as shown in Fig. 1(e). This is consistent with Al atoms being bonded to Si–O ligands with oxygen backbond insertion, as shown in a proposed dissociative chemisorption model in Fig. 7(b). The density of Si and Ge atoms is lower on the SiGe(110) surface than on the SiGe(001) surface; this is consistent with the larger row spacing, after TMA functionalization, for SiGe(110) than for SiGe(001). It is noted that the Al/(Si + Ge) ratio after dosing TMA on $H_2O_2(g)$ functionalized SiGe(110) is at least as large as on SiGe(001); this may be due to the more open structure of the SiGe(110) surface allowing TMA bonding with steric hindrance.

To understand the electronic structures, STS measurements were employed, as shown in Fig. 9. For the 300 °C PDA/25 °C TMA/25 °C H_2O_2/SiGe(001) and 300 °C PDA/25 °C TMA/25 °C H_2O_2/300 °C atomic H/SiGe(110) STS spectra, a black arrow shows that the 25 °C TMA with 300 °C PDA moved the Fermi level closer to the conduction band with a slight decrease of the band bending in valence band edge. This result is consistent with the elimination of the surface dipole by the formation of Al–O–Si bonds. In addition, as shown in Fig. 9, the Fermi level is positioned below the mid-gap; a result consistent with unpinned surfaces with a larger band gap due to the formation of an Al_2O_3 monolayer. Note, the onsets in the experimental (dI/dV)/(I/V) are slightly greater than the fitted curves; this could be indicative of either site-to-site variations in the Fermi level or a small density of band edge states (sometimes called band tails); in either case, the uncertainty in the band gaps is greater than the standard error.

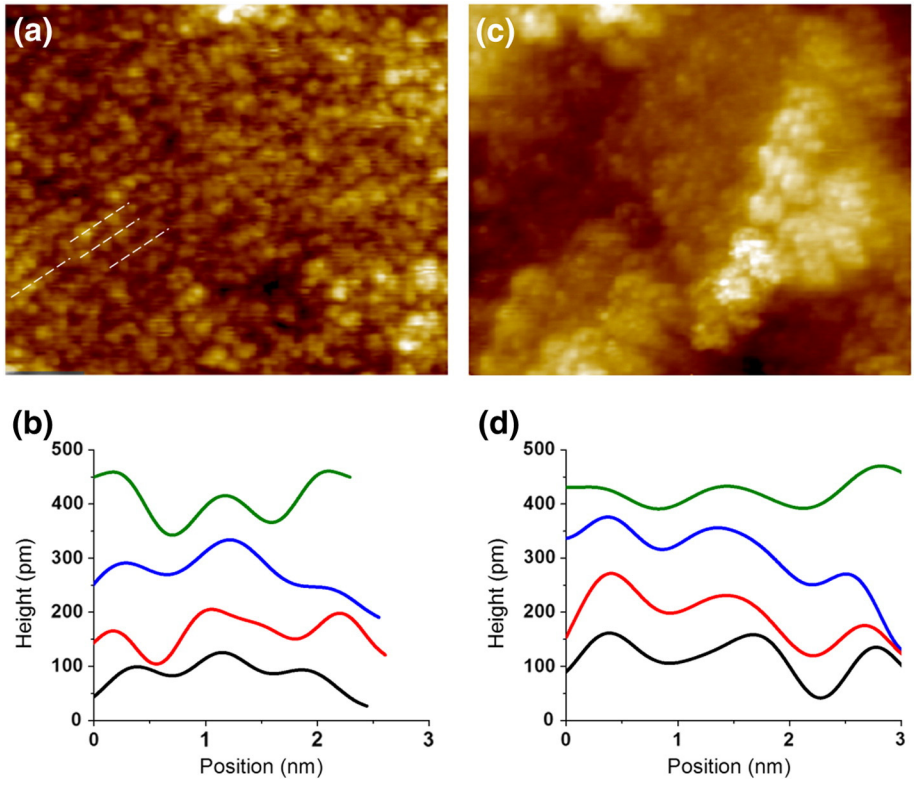

Fig. 8. STM image and line trace of TMA dosed SiGe(001) and (110) surfaces. (a) Filled state STM image (30×25 nm^2, $V_s = -1.8$ V, $I_t = 200$ pA) after a 25 °C TMA dose on 25 °C H_2O_2/SiGe(001) surface followed by 300 °C annealing. (b) Line trace of four different areas on STM image in (a). The average row spacing is 9.0 Å with a standard error of 0.40 Å. (c) STM image (30×25 nm^2, $V_s = -1.8$ V, $I_t = 200$ pA) after a 25 °C TMA dose on 25 °C H_2O_2/atomic H/SiGe(110) surface, followed by 300 °C annealing. (d) Line trace of four different areas on STM image in (c). The average row spacing is 11.8 Å with a standard error of 0.44 Å.

Please cite this article as: S.W. Park, et al., Chemically selective formation of Si–O–Al on SiGe(110) and (001) for ALD nucleation using H2O2(g), Surf. Sci. (2016), http://dx.doi.org/10.1016/j.susc.2016.01.009

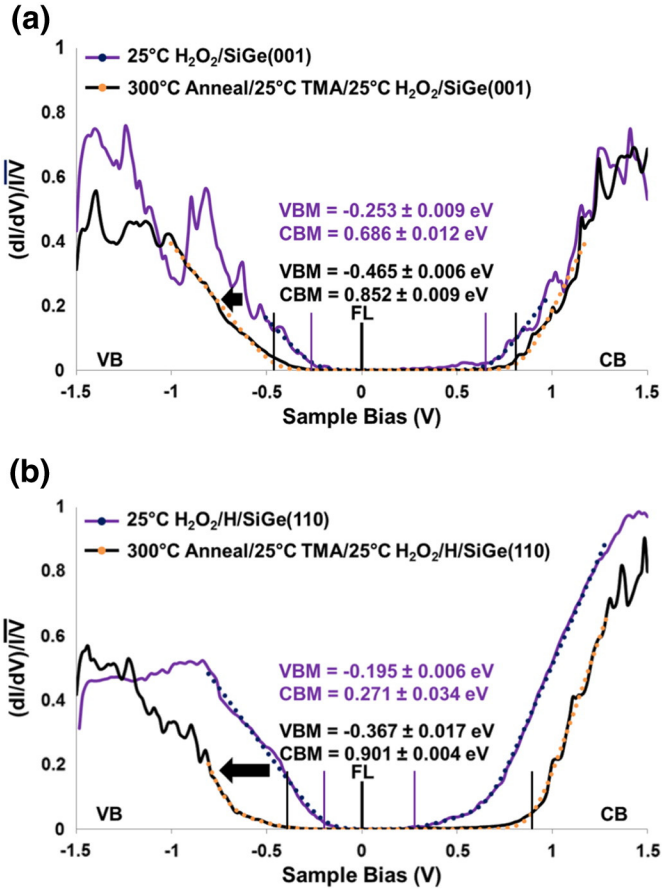

Fig. 9. STS measurements of TMA dosed p-type SiGe(001) and (110) surfaces. (a) The p-type SiGe(001) surface is unpinned after a 25 °C TMA dose on 25 °C H_2O_2/SiGe(001), followed by 300 °C annealing. The black arrow indicates an enlarged band gap due to the formation of Al_2O_3. The range of fitting is −0.5 to 1 V for 25 °C H_2O_2/SiGe(001) surface and is −1 to 1.2 V for 300 °C Anneal/25 °C TMA/25 °C H_2O_2/SiGe(001) surface. (b) The p-type SiGe(110) surface is unpinned after a 25 °C TMA dose on 25 °C H_2O_2/300 °C atomic H/SiGe(110) followed by 300 °C annealing. After a TMA dose, the band gap increases and the Fermi level moves toward mid-gap, consistent with the Si–O–Al bonding having smaller dipoles than the Si–OH bonding. Each STS curve is fit in order to determine the band gaps and Fermi level positions. The range of fitting is −0.8 to 1.3 V for 25 °C H_2O_2/300 °C atomic H/SiGe(110) surface and is −0.8 to 1.3 V for 300 °C Anneal/25 °C TMA/25 °C H_2O_2/300 °C atomic H/SiGe(110) surface.

3.4. Density functional theory simulations

Density functional theory (DFT) modeling was employed to understand the proposed bonding configurations and electronic structures. The DFT modeling was performed for clean and hydroxyl-terminated SiGe(110) surfaces, followed by relaxation. In Fig. 10(a), a DFT model shows a clean unreconstructed SiGe(110) surface terminated by both tri-coordinated Si and Ge atoms with half-filled dangling bonds. Note this is a simplified structure; as shown by Takeuchi and Stekolnikov et al. [51,52], the real structure has additional adatoms consistent with the large spacing of the adatoms in the STM images in Fig. 1(d) and (e); in addition there are multiple nearly degenerate adatoms structures. However, to understand chemical passivation on the surface, the simplified model is sufficient. The DOS of this structure shows states in the band gap region, and the Fermi level of the surface is pinned as shown in Fig. 10(b), which is consistent with the STS measurements in Fig. 2(a). This indicates that the surface is pinned near the mid-gap due to the surface dangling bonds.

DFT and DOS simulations were studied on the SiGe(110) surface passivated with hydroxyls after a $H_2O_2(g)$ dose. In Fig. 11(a), a SiGe(110) surface is terminated with hydroxyls on both Si and Ge atoms after a $H_2O_2(g)$ dose; this result is consistent with the XPS analysis showing both Si–OH and Ge–OH peaks in Fig. 3(a) and (b). In contrast to a clean SiGe(110) surface, the DOS of the hydroxyl-terminated SiGe(110) surface demonstrates the elimination of the states in the band gap region. This is consistent with the STS results showing no mid-gap defect states after a $H_2O_2(g)$ dose in Fig. 5. It is anticipated that a similar phenomenon should be demonstrated on an unpinned SiGe(110) surface with H termination after an atomic H dose, as shown in Fig. 2(b).

4. Conclusion

Chemical, topological, and electronic structures of SiGe(110) and (001) surfaces were compared and analyzed using *in-situ* XPS, STM, and STS. The clean SiGe(110) is terminated with adatoms with a low surface order, while the clean SiGe(001) surface is terminated with Ge dimers with a uniform and well-ordered structure. STS measurements verified that the clean (110) surface is pinned near the mid-gap by adatom dangling bonds, while the clean (001) surface is unpinned. The sputter-cleaned SiGe(110) surface was dosed at 300 °C with a 3600 L dose of atomic H to passivate the adatom dangling bonds. STS measurements demonstrated that the atomic H-dosed SiGe(110)

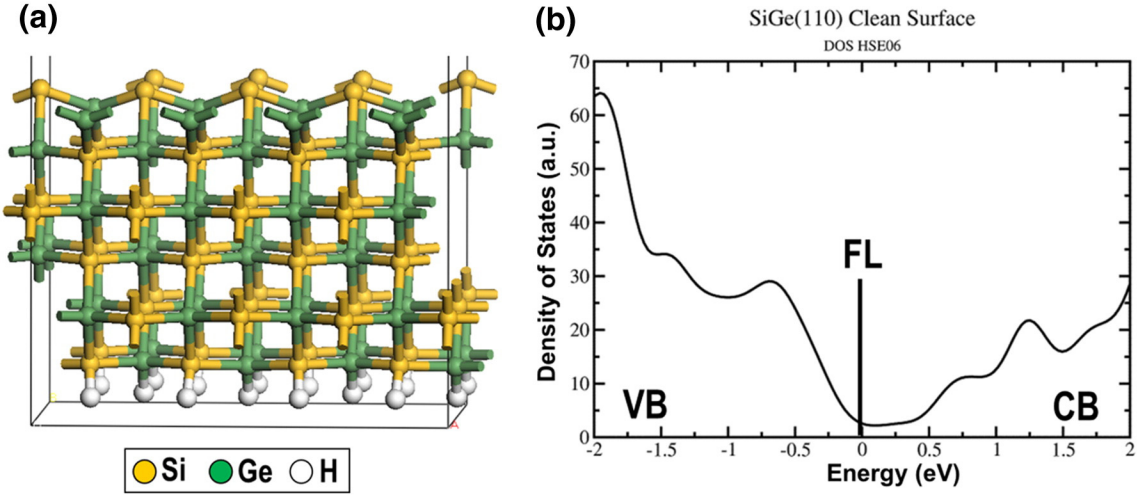

Fig. 10. DFT Model and HSE06 DOS of a clean SiGe(110) surface. (a) The clean SiGe(110) surface is terminated with Si and Ge atoms. S — yellow, Ge — green, and H — white. (b) The DOS shows states in the band gap, and the clean SiGe(110) surface is pinned. (For interpretation of the references to color in this figure legend, the reader is referred to the web version of this article.)

Please cite this article as: S.W. Park, et al., Chemically selective formation of Si–O–Al on SiGe(110) and (001) for ALD nucleation using H2O2(g), Surf. Sci. (2016), http://dx.doi.org/10.1016/j.susc.2016.01.009

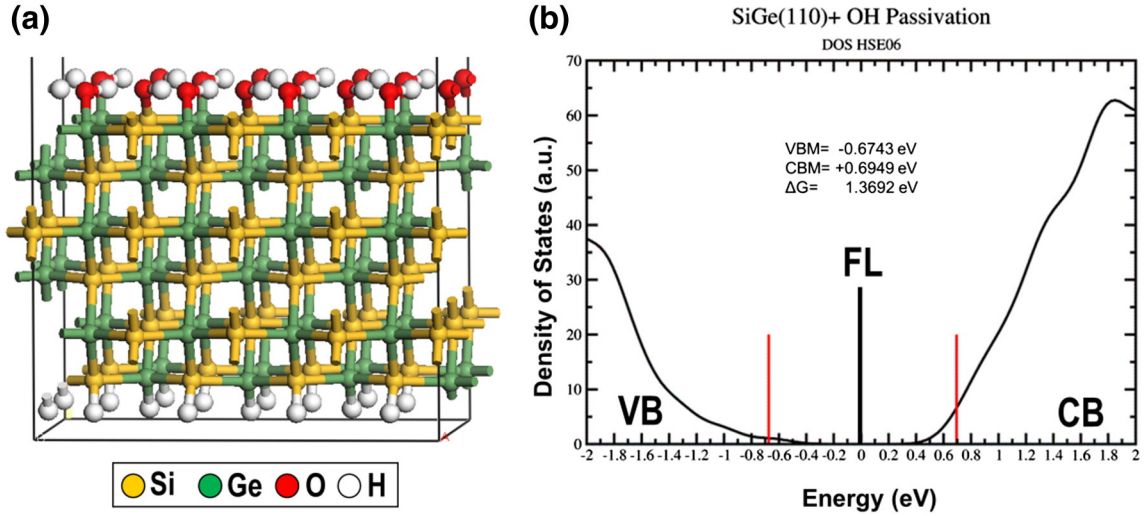

Fig. 11. DFT Model and HSE06 DOS of H_2O_2 dosed SiGe (110) surface. (a) The SiGe(110) surface is terminated with hydroxyls on both Si and Ge atoms after a $H_2O_2(g)$ dose. Si — yellow, Ge — green, O — red, and H — white. (b) The DOS shows the elimination of states in the band gap after the passivation by hydroxyls via a $H_2O_2(g)$ dose. (For interpretation of the references to color in this figure legend, the reader is referred to the web version of this article.)

surface is consistent with unpinning, with a Fermi level near the valence band due to the passivation of the surface adatoms. The 300 °C atomic H dose induced a partial Si segregation to the SiGe surfaces because the bond strength of Si–H is larger than that of Ge–H. The Si segregated SiGe(110) and (001) surfaces should be ideal for FinFET structures due to the low defect density of Si/high-*k* dielectric interfaces after a forming gas annealing [64]. It is known that Si termination passivates defects on Ge PMOS transistors that result in a lower D_{it} [12]. The 300 °C atomic H/SiGe(110) and (001) surfaces were dosed at 25 °C with saturation doses of $H_2O_2(g)$, leaving the SiGe surface terminated with an ordered monolayer of mainly $Si–O_xH_y$ sites on SiGe(110), and only $Ge–O_xH_y$ sites on SiGe(001) surfaces [13]. TMA was subsequently dosed at 25 °C on the 25 °C H_2O_2/300 °C atomic H/SiGe(110) and 25 °C H_2O_2/SiGe(001) surfaces. The surfaces were annealed at temperatures up to 300 °C, and XPS measurements verified complete Si/Ge place exchange, so that only Al–O–Si bonds are formed on both (110) and (001). This indicates the ability of Si to diffuse to the oxide/SiGe interface and displace Ge, even at modest temperatures. STS measurements indicated that the Fermi levels on both surfaces were consistent with unpinning, leaving an electrically passive, ordered layer, which serves as an ideal template for further high-*k* ALD.

Acknowledgments

This work was supported in part by the Center for Low Energy Systems Technology (LEAST), one of six centers of STARnet, a Semiconductor Research Corporation program sponsored by MARCO and DARPA, NSF DMR 1207213, and Applied Materials. The SiGe wafers were provided by GLOBALFOUNDRIES.

Supplementary data

Supplementary data to this article can be found online at http://dx.doi.org/10.1016/j.susc.2016.01.009.

References

[1] H. Xuejue, et al., Sub 50-nm FinFET: PMOS, IEDM'99, Tech. Dig. Int. (1999) 67.
[2] D. Hisamoto, et al., FinFET—a self-aligned double-gate MOSFET scalable to 20 nm, IEEE T. Electron Dev. 47 (2000) 2320.
[3] H. Xuejue, et al., Sub 50-nm P-channel FinFET, IEEE T. Electron Dev. 48 (2001) 880.
[4] Y. Bin, et al., FinFET scaling to 10 nm gate length, IEDM '02, Tech. Dig. Int. 251–254 (2002).
[5] S. Datta, et al., High mobility Si/SiGe strained channel MOS transistors with HfO_2/TiN gate stack, 2003 IEDM'03, Tech. Dig. Int. 653–656 (2003).
[6] S. Datta, et al., Advanced Si and SiGe strained channel NMOS and PMOS transistors with high-K/metal-gate stack, Proc. of 2004 BCTM, 2004 194.
[7] T. Ghani, et al., A 90 nm high volume manufacturing logic technology featuring novel 45 nm gate length strained silicon CMOS transistors, 2003 IEDM'03, Tech. Dig. Int. (2003) (11.6.1–11.6.3).
[8] T. Mizuno, S. Takagi, N. Sugiyama, H. Satake, A. Kurobe, A. Toriumi, Electron and hole mobility enhancement in strained-Si MOSFET's on SiGe-on-insulator substrates fabricated by SIMOX technology, IEEE Electr. Device L. 21 (2000) 230.
[9] T. Mizuno, N. Sugiyama, H. Satake, S. Takagi, Advanced SOI-MOSFETs with strained-Si channel for high speed CMOS — electron/hole mobility enhancement, 2000 Symposium on Vlsi Technology, Digest of Technical Papers 2000, p. 210.
[10] M.L. Lee, et al., Strained Ge channel p-type metal-oxide-semiconductor field-effect transistors grown on $Si_{1-x}Ge_x$/Si virtual substrates, Appl. Phys. Lett. 79 (2001) 3344.
[11] K.J. Kuhn, A. Murthy, R. Kotlyar, M. Kuhn, Past, present and future: SiGe and CMOS transistor scaling SiGe, Ge, and related compounds 4, Mater. Process. Devices 33 (6) (2010) 3.
[12] M. Caymax, et al., The influence of the epitaxial growth process parameters on layer characteristics and device performance in Si-passivated Ge pMOSFETs, J. Electrochem. Soc. 156 (2009) H979.
[13] T. Kaufman-Osborn, E.A. Chagarov, S.W. Park, B. Sahu, S. Siddiqui, A.C. Kummel, Atomic imaging and modeling of passivation, functionalization, and atomic layer deposition nucleation of the SiGe(001) surface via $H_2O_2(g)$ and trimethylaluminum dosing, Surf. Sci. 630 (2014) 273.
[14] D. Kuzum, et al., Ge-interface engineering with ozone oxidation for low interface-state density, IEEE Electr. Device L. 29 (2008) 328.
[15] J.S. Lee, T. Kaufman-Osborn, W. Melitz, S. Lee, A. Kummel, Effect of H_2O chemisorption on passivation of Ge(100) surface studied by scanning tunneling microscopy, Surf. Sci. 605 (2011) 1583.
[16] T. Kaufman-Osborn, E.A. Chagarov, A.C. Kummel, Atomic imaging and modeling of $H_2O_2(g)$ surface passivation, functionalization, and atomic layer deposition nucleation on the Ge(100) surface, J. Chem. Phys. 140 (2014) 204708.
[17] H. Takeuchi, T. Matsuura, J. Murota, Contribution of ions and radicals in etching of $Si_{1-x}Ge_x$ epitaxial films using an electron-cyclotron-resonance chlorine plasma, Appl. Phys. Lett. 77 (2000) 1828.
[18] Y. Zhang, G.S. Oehrlein, E. de Frésart, J.W. Corbett, Reactive ion etching of SiGe alloys using CF_2Cl_2, J. Appl. Phys. 71 (1992) 1936.
[19] T.D. Bestwick, G.S. Oehrlein, Y. Zhang, G.M.W. Kroesen, E. de Frésart, Reactive ion etching of SiGe alloys using HBr, Appl. Phys. Lett. 59 (1991) 336.
[20] G.S. Oehrlein, G.M.W. Kroesen, E. de Frésart, Y. Zhang, T.D. Bestwick, Studies of the reactive ion etching of SiGe alloys, J. Vac. Sci. Technol. A 9 (1991) 768.
[21] E. Rudkevich, F. Liu, D.E. Savage, T.F. Kuech, L. McCaughan, M.G. Lagally, Hydrogen induced Si surface segregation on Ge-covered Si(001), Phys. Rev. Lett. 81 (1998) 3467.
[22] K. Nakagawa, A. Nishida, Y. Kimura, T. Shimada, Effect of atomic and molecular-hydrogen irradiation on Ge surface segregation during Si molecular-beam epitaxy, Jpn. J. Appl. Phys. 2 (33) (1994) L1331.
[23] M. Copel, R.M. Tromp, Are bare surfaces detrimental in epitaxial-growth, Appl. Phys. Lett. 58 (1991) 2648.
[24] D.A. Grutzmacher, et al., Ge segregation in SiGe/Si heterostructures and its dependence on deposition technique and growth atmosphere, Appl. Phys. Lett. 63 (1993) 2531.
[25] Y.J. Zheng, P.F. Ma, J.R. Engstrom, Etching by atomic hydrogen of Ge overlayers on Si(100), J. Appl. Phys. 90 (2001) 3614.

Please cite this article as: S.W. Park, et al., Chemically selective formation of Si–O–Al on SiGe(110) and (001) for ALD nucleation using H2O2(*g*), Surf. Sci. (2016), http://dx.doi.org/10.1016/j.susc.2016.01.009

[26] J.Y. Lee, S.J. Jung, J.Y. Maeng, Y.E. Cho, S. Kim, S.K. Jo, Atomic-scale structural evolution of Ge(100) surfaces etched by H and D, Appl. Phys. Lett. 84 (2004) 5028.
[27] A.P. Webb, S. Vepřek, Recativity of solid silicon with hydrogen under conditions of a low pressure plasma, Chem. Phys. Lett. 62 (1979) 173.
[28] A. Stesmans, Passivation of P_{b0} and P_{b1} interface defects in thermal (100) Si/SiO_2 with molecular hydrogen, Appl. Phys. Lett. 68 (1996) 2076.
[29] M.L. Reed, J.D. Plummer, Chemistry of $Si–SiO_2$ interface trap annealing, J. Appl. Phys. 63 (1988) 5776.
[30] K.L. Brower, Passivation of paramagnetic $Si–SiO_2$ interface states with molecular-hydrogen, Appl. Phys. Lett. 53 (1988) 508.
[31] K.L. Brower, Kinetics of H_2 passivation of P_b centers at the (111) $Si–SiO_2$ interface, Phys. Rev. B 38 (1988) 5657.
[32] S.L. Manatt, M.R.R. Manatt, On the analyses of mixture vapor pressure data: the hydrogen peroxide/water system and its excess thermodynamic functions, Chem. Eur. J. 10 (2004) 6540.
[33] R.M. Feenstra, J.A. Stroscio, A.P. Fein, Tunneling spectroscopy of the Si(111) 2×1 surface, Surf. Sci. 181 (1987) 295.
[34] R.M. Feenstra, Scanning tunneling spectroscopy, Surf. Sci. 299–300 (1994) 965.
[35] R.M. Feenstra, J.Y. Lee, M.H. Kang, G. Meter, K.H. Rieder, Band gap of the Ge(111)c(2×8) surface by scanning tunneling spectroscopy, Phys. Rev. B 73 (2006) 035310.
[36] R.M. Feenstra, Tunneling spectroscopy of the (110)surface of direct-gap III–V semiconductors, Phys. Rev. B 50 (1994) 4561.
[37] G. Kresse, J. Hafner, Ab initio molecular dynamics for liquid metals, Phys. Rev. B 47 (1993) 558.
[38] G. Kresse, J. Hafner, Ab initio molecular-dynamics simulation of the liquid-metal–amorphous-semiconductor transition in germanium, Phys. Rev. B 49 (1994) 14251.
[39] G. Kresse, J. Furthmüller, Efficiency of ab-initio total energy calculations for metals and semiconductors using a plane-wave basis set, Comp. Mater. Sci. 6 (1996) 15.
[40] G. Kresse, J. Furthmuller, Efficient iterative schemes for ab initio total-energy calculations using a plane-wave basis set, Phys. Rev. B 54 (1996) 11169.
[41] P.E. Blöchl, Projector augmented-wave method, Phys. Rev. B 50 (1994) 17953.
[42] G. Kresse, D. Joubert, From ultrasoft pseudopotentials to the projector augmented-wave method, Phys. Rev. B 59 (1999) 1758.
[43] J.P. Perdew, K. Burke, M. Ernzerhof, Generalized gradient approximation made simple, Phys. Rev. Lett. 77 (1996) 3865.
[44] J. Heyd, G.E. Scuseria, M. Ernzerhof, Hybrid functionals based on a screened Coulomb potential, J. Chem. Phys. 118 (2003) 8207.
[45] J. Heyd, G.E. Scuseria, Efficient hybrid density functional calculations in solids: assessment of the Heyd–Scuseria–Ernzerhof screened Coulomb hybrid functional, J. Chem. Phys. 121 (2004) 1187.
[46] J. Heyd, G.E. Scuseria, M. Ernzerhof, Hybrid functionals based on a screened Coulomb potential, J. Chem. Phys. 124 (2006) 219906.
[47] A.V. Krukau, O.A. Vydrov, A.F. Izmaylov, G.E. Scuseria, Influence of the exchange screening parameter on the performance of screened hybrid functionals, J. Chem. Phys. 125 (2006) 224106.
[48] D.J. Godbey, M.G. Ancona, Ge profile from the growth of SiGe buried layers by molecular-beam epitaxy, Appl. Phys. Lett. 61 (1992) 2217.
[49] D.J. Godbey, M.G. Ancona, Concentration-dependence of Ge segregation during the growth of a SiGe buried layer, J. Vac. Sci. Technol. B 11 (1993) 1392.
[50] G.G. Jernigan, P.E. Thompson, C.L. Silvestre, Quantitative measurements of Ge surface segregation during SiGe alloy growth, Surf. Sci. 380 (1997) 417.
[51] N. Takeuchi, Bond conserving rotation, adatoms and rest atoms in the reconstruction of Si(110) and Ge(110) surfaces: a first principles study, Surf. Sci. 494 (2001) 21.
[52] A.A. Stekolnikov, J. Furthmuller, F. Bechstedt, Structural elements on reconstructed Si and Ge(110) surfaces, Phys. Rev. B 70 (2004) 045305.
[53] A.J. Mayne, A.R. Avery, J. Knall, T.S. Jones, G.A.D. Briggs, W.H. Weinberg, An STM study of the chemisorption of C_2H_4 on Si(001) (2×1), Surf. Sci. 284 (1993) 247.
[54] C.C. Hobbs, et al., Fermi-level pinning at the polysilicon/metal-oxide interface — part II, IEEE Trans. Electron Devices 51 (2004) 978.
[55] P.D. Kirsch, C.S. Kang, J. Lozano, J.C. Lee, J.G. Ekerdt, Electrical and spectroscopic comparison of HfO_2/Si interfaces on nitrided and un-nitrided Si(100), J. Appl. Phys. 91 (2002) 4353.
[56] M. Edmonds, et al., Passivation of InGaAs(001)-(2×4) by self-limiting chemical vapor deposition of a silicon hydride control layer, J. Am. Chem. Soc. 137 (2015) 8526.
[57] Y. Sun, Z. Liu, S.Y. Sun, P. Pianetta, The effectiveness of HCl and HF cleaning of $Si_{0.85}Ge_{0.15}$ surface, J. Vac. Sci. Technol. A 26 (2008) 1248.
[58] Y.-R. Luo, Comprehensive Handbook of Chemical Bond Energies, CRC Press, Boca Raton, 2007.
[59] F. Bensliman, Y. Sawada, K. Tsujino, M. Matsumura, Oxidation of atomically flat and hydrogen-terminated Si(111) surfaces by hydrogen peroxide, J. Electrochem. Soc. 154 (2007) F102.
[60] W.C. O'Mara, R.B. Herring, L.P. Hunt, Handbook of Semiconductor Silicon Technology, Noyes Publications, Park Ridge, NJ, 1990.
[61] J.H. Scofield, Hartree–Slater subshell photoionization cross-sections at 1254 and 1487 eV, J. Electron Spectrosc. 8 (1976) 129.
[62] M.P. Seah, W.A. Dench, Quantitative electron spectroscopy of surfaces: a standard data base for electron inelastic mean free paths in solids, Surf. Interface Anal. 1 (1979) 2.
[63] T.J. Grassman, S.R. Bishop, A.C. Kummel, An atomic view of Fermi level pinning of Ge(100) by O_2, Surf. Sci. 602 (2008) 2373.
[64] K. Onishi, et al., Improvement of surface carrier mobility of HfO_2/MOSFETs by high-temperature forming gas annealing, IEEE Trans. Electron Devices 50 (2003) 384.

Please cite this article as: S.W. Park, et al., Chemically selective formation of Si–O–Al on SiGe(110) and (001) for ALD nucleation using H2O2(g), Surf. Sci. (2016), http://dx.doi.org/10.1016/j.susc.2016.01.009